

Effects of hyperons in binary neutron star mergers

Yuichiro Sekiguchi, Kenta Kiuchi, Koutarou Kyutoku, and Masaru Shibata
Yukawa Institute for Theoretical Physics, Kyoto University, Kyoto 606-8502, Japan

Numerical simulations for the merger of binary neutron stars are performed in full general relativity incorporating both nucleonic and hyperonic finite-temperature equations of state (EOS) and neutrino cooling for the first time. It is found that even for the hyperonic EOS, a hypermassive neutron star is first formed after the merger for the typical total mass $\approx 2.7M_\odot$, and subsequently collapses to a black hole (BH). It is shown that hyperons play a substantial role in the post-merger dynamics, torus formation around the BH, and emission of gravitational waves (GWs). In particular, the existence of hyperons is imprinted in GWs. Therefore, GW observations will provide a potential opportunity to explore the composition of the neutron star matter.

PACS numbers: 04.25.Dm, 04.30.-w, 04.40.Dg

Introduction: The properties of the neutron star (NS) matter, in particular its equation of state (EOS), are still poorly understood. In recent years, the influence of non-nucleonic degrees of freedom, such as hyperons, meson condensations, and quarks, on properties of the NS matter has been discussed extensively [1, 2]. From an energetic point of view, eventual appearances of these *exotic* phases seem to be natural because of the Pauli principle: the chemical potential for neutrons will eventually exceed that of exotic particles at some high densities. However, it is currently uncertain at which density and temperature these exotic particles appear, because their interactions are not accurately known. Generally speaking, presence of such exotic particles results in softening of EOS. This effect reduces the maximum mass of NS. The recent mass measurement of PSR J1614-2230 ($M_{\text{J1614-2230}} = 1.97 \pm 0.04M_\odot$) [3] gave a strong impact on the properties of the NS matter, indicating that stiff EOSs are preferable. However, it does not still constrain the existence of exotic particles in NS [2, 4].

There have been a number of numerical studies exploring effects of such exotic phases on astrophysical phenomena [5–10], aiming at extracting information of the NS matter. In the context of stellar core collapse, effects of hadron-quark phase transition on dynamics and neutrino signals were studied in [5, 6] using the MIT bag model for the quark phase. The hadron-quark transition is imprinted in the neutrino signals, and in special conditions, it could generate a second shock wave which triggers a delayed supernova explosion [6]. Sumiyoshi et al. [7] studied the effects of hyperons in failed supernovae adopting an EOS developed in [11]. By contrast, effects of the exotic particles on dynamics and gravitational waves (GWs) from binary neutron stars (BNS) mergers and hypermassive neutron stars (HMNS) subsequently formed have not been studied in detail (but see recent studies in [8, 9]), although the coalescence of BNS is one of the most promising sources for next-generation kilo-meter-size GW detectors [12].

Among exotic particles, Λ hyperons are believed to appear first in (cold) NS around the rest-mass density of $\rho \sim 2\text{--}3\rho_{\text{nuc}}$ [1, 11], where $\rho_{\text{nuc}} \approx 2.8 \times 10^{14}\text{g/cm}^3$ is the nuclear matter density. In this *Letter*, we

present the first results of numerical-relativity simulations for the BNS merger performed incorporating a finite-temperature EOS including contributions of Λ hyperons [14] (Hyp-EOS). We ignore the contributions of Σ hyperons because recent experiments suggest that Σ hyperons feel a repulsive potential [13] while Λ hyperons feel an attractive potential [11], and hence, Λ hyperons are likely to appear first and to be dominant. In the following, we report the effects of Λ hyperons on merger dynamics, black hole (BH) formation, neutrino signals, and gravitational waveforms. We show that the emergence of Λ hyperons is imprinted in GWs from the HMNS.

Setting of numerical simulations: Numerical simulations in full general relativity are performed using the same method and formulation as in [15, 16]: Einstein's equations are solved in the so-called Baumgarte-Shapiro-Shibata-Nakamura (BSSN)-puncture formulation [17] with dynamical gauge conditions for the lapse function and the shift vector; a fourth-order finite differencing in space and a fourth-order Runge-Kutta time integration are used; a conservative shock capturing scheme with third-order accuracy in space and fourth-order accuracy in time is employed for solving hydrodynamic equations. In addition to the ordinary hydrodynamic equations, we solve evolution equations for the neutrino (Y_ν), electron (Y_e), and total lepton (Y_l) fractions per baryon, taking account of weak interaction processes and neutrino cooling employing a general relativistic leakage scheme for electron neutrinos (ν_e), electron antineutrinos ($\bar{\nu}_e$), and other types (μ/τ) of neutrinos (ν_x) [18, 19].

The results with Hyp-EOS are compared with those with a finite-temperature nucleonic EOS [20] (Shen-EOS). The maximum mass of zero-temperature spherical NS for Hyp-EOS is $M_{\text{max,Hyp}} \approx 1.8M_\odot$. This is smaller than that for Shen-EOS, $M_{\text{max,Shen}} \approx 2.2M_\odot$. Although $M_{\text{max,Hyp}}$ is slightly smaller than $M_{\text{J1614-2230}}$, Hyp-EOS deserves employing to explore the impact of hyperons on the BNS merger, because it can be a viable EOS of the NS matter not in extremely high densities and hence for studying the evolution of the HMNS that do not have the extremely high densities for most of their lifetime. Simulations with finite-temperature EOSs with exotic phases which can produce a stable NS with mass larger than

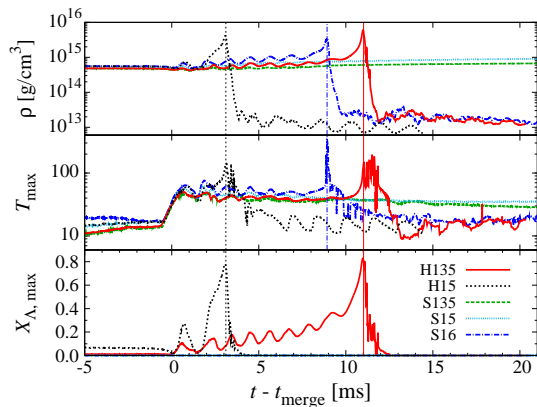


FIG. 1: Maximum rest-mass density, maximum matter temperature, and maximum mass fraction of hyperons as functions of time for H135 (solid red), H15 (dotted black), S135 (dashed green), S15 (short-dotted cyan), and S16 (dashed-dotted blue). The vertical thin lines show the time at which a BH is formed.

$M_{J1614-2230}$ should be performed in the future studies.

Numerical simulations are performed in a non-uniform grid [15, 16]. The inner domain is composed of a finer uniform grid and the outer domain of a coarser nonuniform grid. The grid resolution in the inner zone is chosen so that the major diameter of each neutron star in the inspiral orbit is covered by 60 and 80 grid points for low- and high-resolution runs, respectively, and we confirm that the convergence is achieved except for stochastic behaviors due to convective motions. Outer boundaries are located in a local wave zone (at ≈ 560 – 600 km along each coordinate axis which is longer than gravitational wavelengths in the inspiral phase). During the simulations, we check the conservation of baryon rest-mass, total gravitational mass, and total angular momentum, and find that the errors are within 0.2%, 1%, and 2%, respectively, for the high-resolution runs.

This *Letter* focuses on the merger of equal-mass BNS. The gravitational mass of single NS in isolation is $M_{\text{NS}} = 1.35$ and $1.5M_{\odot}$ for Hyp-EOS (referred to as H135 and H15). We perform simulations with the initial condition of about 3–4 orbits before the onset of the merger until the system relaxes to a quasistationary state. Quasiequilibrium states of BNS are prepared as the initial conditions, as in [21]. We compare the simulation results with those for Shen-EOS with $M_{\text{NS}} = 1.35$, 1.5 , and $1.6M_{\odot}$ (referred to as S135, S15, and S16) obtained in [15]. We do not take account of magnetic fields in the present simulations, which may play a role in the late-phase evolution after the onset of the merger [22].

Numerical results: Figure 1 plots the evolution of maximum rest-mass density, ρ_{max} , maximum temperature, T_{max} , and maximum mass fraction of hyperons, $X_{\Lambda, \text{max}}$ as functions of $t - t_{\text{merge}}$ where t_{merge} is an approximate onset time of the merger. Before the merger ($t < t_{\text{merge}}$), ρ_{max} and T_{max} for H135 and H15 agree well with those

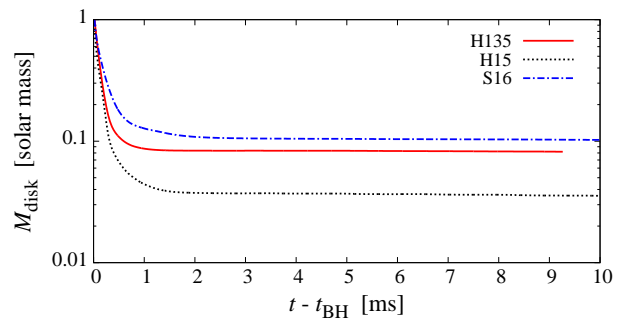


FIG. 2: The torus mass as a function of time after the BH formation for H135 (solid red), H15 (dotted black), and S16 (dashed-dotted blue).

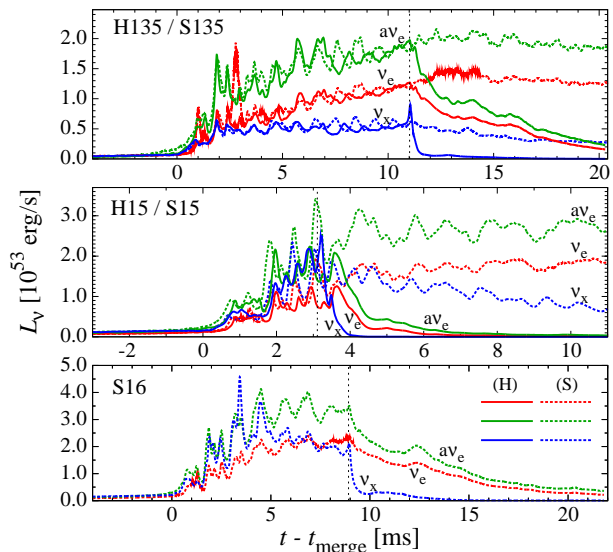


FIG. 3: Neutrino luminosities for H135 and S135 (top), H15 and S15 (middle), and S16 (bottom). The dotted vertical lines show the time at which a BH is formed. The solid and dashed curves correspond to the result with the Hyp-EOS and Shen-EOS, respectively.

for the corresponding Shen-EOS model S135 and S15, because $X_{\Lambda, \text{max}}$ in this phase is small as $O(10^{-2})$ and effects of hyperons on dynamics are not significant. After the merger sets in ($t > t_{\text{merge}}$), on the other hand, $X_{\Lambda, \text{max}}$ increases to be $\gtrsim 0.1$ in accordance with the increase in ρ_{max} , and hyperons play a substantial role in the post-merger dynamics and emission of GWs (see below).

Although the total mass, M , is larger than the maximum mass of the zero-temperature spherical NS for all the models, a HMNS is formed after the merger, supported by the centrifugal force and thermal contributions to the pressure [9, 15]. They subsequently contract by emission of GWs, and for H135, H15, and S16, they collapse to a black hole (BH) at $t = t_{\text{BH}}$ where $t_{\text{BH}} - t_{\text{merge}} \approx 11.0$, 3.1 , and 8.9 ms, respectively. The HMNS for S135 and S15 will not collapse to a BH in a cooling time, $t_{\text{cool}} \equiv E_{\text{th}}/L_{\nu} \sim 2$ – 3 s, where E_{th} is total thermal energy and L_{ν} is total neutrino luminosity [15].

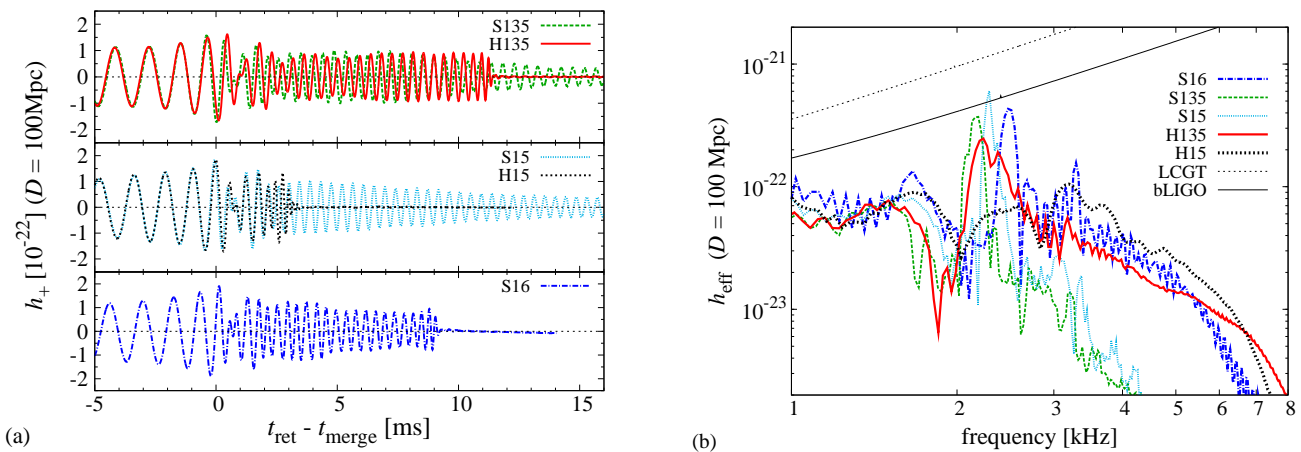


FIG. 4: (a) GWs observed along the axis perpendicular to the orbital plane for the hypothetical distance to the source $D = 100$ Mpc. (b) The effective amplitude of GWs defined by $0.4f|h(f)|$ as a function of frequency for $D = 100$ Mpc. The noise amplitudes of a broadband configuration of Advanced Laser Interferometer Gravitational wave Observatories (bLIGO), and Large-scale Cryogenic Gravitational wave Telescope (LCGT) are shown together.

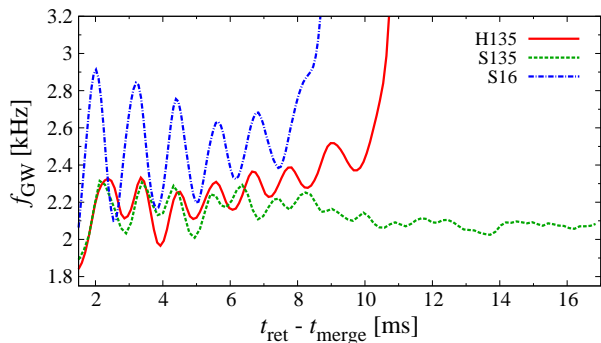


FIG. 5: $f_{\text{GW}}(t)$ in the HMNS phase, smoothed by a weighted spline, for H135 (solid red), S135 (dashed green), and S16 (dashed-dotted blue).

After the BH formation for H135, H15, and S16, an accretion torus is formed around the BH. Figure 2 plots the torus mass, M_{torus} , as a function of time. M_{torus} in a quasistationary state is ≈ 0.082 , 0.035 , and $0.10M_{\odot}$ for H135, H15, and S16, respectively, with $\rho_{\text{max}} \approx 10^{13}$ g/cm³ (see Fig. 1). For H15, M_{torus} is smaller than those for other models because angular momentum is not significantly transported in the outer region of the HMNS due to its short lifetime. Interestingly, M_{torus} is smaller for H135 than that for S16 in spite of the longer lifetime of the HMNS. This is likely because the HMNS for H135 just before the BH formation is more compact than that for S16. Our results suggest that the emergence of non-nucleonic degrees of freedom such as hyperons would have a negative impact for driving a short-gamma ray burst for which formation of a massive torus is preferred [23].

Figure 3 plots neutrino luminosities as functions of time. Electron antineutrinos are dominantly emitted for all the models as found in the previous studies [15, 24]. For H135, H15, and S16, the μ/τ neutrino luminosity shows a spike around $t \approx t_{\text{BH}}$ because high temperature

is achieved as a result of compression. Although T_{max} is very large as $\gtrsim 100$ MeV, the peak amplitude is moderate because of long diffusion timescale of neutrinos due to the high density. Soon after the BH formation, μ/τ neutrino luminosity steeply decreases because high temperature regions are swallowed into the BH, while luminosities of electron neutrinos and antineutrinos decrease only gradually because these neutrinos are emitted via charged-current processes from the massive accretion torus [15]. These features in neutrino luminosities are quantitatively the same for Hyp-EOS and Shen-EOS models, and hence, it would be difficult to extract information of the NS matter only from the neutrino signal.

Figure 4(a) plots the plus mode (h_+) of GWs as a function of $t_{\text{ret}} - t_{\text{merge}}$ where t_{ret} is the retarded time, extracted from the metric in the local wave zone. The GW amplitude is $h_+ \lesssim 2 \times 10^{-22}$ for a source at a distance $D = 100$ Mpc. GWs from the inspiral phase (for $t_{\text{ret}} \lesssim t_{\text{merge}}$) agree well with each other for the models with Hyp-EOS and Shen-EOS for the same mass. On the other hand, quasi-periodic GWs from the HMNS (for $t_{\text{ret}} \gtrsim t_{\text{merge}}$) show differences. First, the amplitude of quasi-periodic GWs damps steeply at the BH formation for H135 and H15. This is because the HMNS collapse to a BH due to the softening of the EOS before relaxing to a stationary spheroid. Second, the characteristic GW frequency, f_{GW} , *increases* with time for Hyp-EOS models. These facts are clearly observed in the effective amplitude [see Fig. 4(b)] defined by $h_{\text{eff}} \equiv 0.4f|h(f)|$ where $h(f)$ is the Fourier transform of $h_+ - ih_{\times}$ with h_{\times} being the cross mode and the factor 0.4 comes from taking average in terms of direction to the source and rotational axis of the HMNS. Reflecting a shorter lifetime of the HMNS in Hyp-EOS models, the peak amplitude of $h_{\text{eff}}(f)$ is smaller, in particular for H15 where the HMNS survives only for a short period ~ 3 ms. Reflecting the shift of the characteristic frequency, the prominent peak in the GW

spectra for Hyp-EOS models (H135 and H15) is broadened. We here note that the lifetime of the HMNS is longer for H135 than that for S16. The reason for this broadening of the peak is described as follows in more detail.

In the case that hyperons are absent, the HMNS slightly contract simply due to the angular momentum loss (weakening centrifugal force) via GW emission. By contrast, in the case that hyperons are present, X_Λ increases with the contraction of the HMNS, resulting in the relative reduction of the pressure. As a result, the HMNS further contract. Recent studies showed that f_{GW} is associated with the frequency of f -mode which is approximately proportional to $\sqrt{M_{\text{H}}/R_{\text{H}}^3}$ where M_{H} and R_{H} are the mass and radius of the HMNS [10, 25]. This indicates that f_{GW} should increase with time. To see that this is indeed the case, we show $f_{\text{GW}}(\equiv d\phi_{\text{NP}}/dt)$ calculated from a Weyl scalar $\Psi_4 \equiv \Psi e^{-i\phi_{\text{NP}}}$ in the HMNS phase for H135, S135, and S16 in Fig. 5. It is clearly seen that the mean value of f_{GW} in the HMNS phase is approximately constant for Shen-EOS models; $f_{\text{GW}} \approx 2.1$ and 2.5 kHz for S135 and S16, respectively. By contrast, f_{GW} for H135 increases with time (from $f_{\text{GW}} \approx 2.0$ kHz at $t_{\text{ret}} - t_{\text{merge}} = 2$ ms to ≈ 2.5 kHz at $t_{\text{ret}} - t_{\text{merge}} = 10$ ms) as the HMNS becomes compact.

Our results raise a caution that one should be careful when using the peak frequency of the GW spectrum to extract information of the NS matter, because f_{GW} evolves with time for Hyp-EOS models. This makes it ambiguous to determine f_{GW} and to relate f_{GW} with the HMNS structure. Our results rather suggest a possibility that the emergence of hyperons may be captured from

the evolution of the characteristic frequency of GW and the peak width of the GW spectra. Accompanied with this broadening, the peak amplitude in h_{eff} decreases by a factor of a few.

Summary: We have reported effects of hyperons on the BNS merger in numerical-relativity simulations incorporating finite-temperature, both hyperonic and nucleonic EOS, microphysical processes, and neutrino cooling. We showed that for the adopted hyperonic EOS, a BH is not promptly formed and a HMNS is first formed for the typical total mass of BNS ($\approx 2.7M_\odot$), as in the nucleonic Shen-EOS [15]. The HMNS subsequently collapse to a BH and a massive torus is formed around the BH. The torus mass for the hyperonic EOS is smaller than that for the nucleonic EOS. We further showed that for the hyperonic EOS, the characteristic frequency of GWs, f_{GW} , from the HMNS increases by a factor of ~ 20 – 30% during their evolution via GW emission, by contrast with that for the nucleonic EOS in which f_{GW} is approximately constant. Although the hyperonic EOS adopted in this *Letter* has some limitations that it only takes Λ hyperons into account and that it cannot produce a stable NS with mass $M_{\text{J1614-2230}}$, we believe from our results that it will be possible to constrain the composition of the NS matter via observation of GW from the HMNS.

Acknowledgments: Numerical simulations were performed on SR16000 at YITP of Kyoto University and on SX9 and XT4 at CfCA of NAOJ. This work was supported by Grant-in-Aid for Scientific Research (21018008, 21105511, 21340051, 22740178, 23740160), Grant-in-Aid on Innovative Area (20105004), and HPCI Strategic Program of Japanese MEXT.

-
- [1] J. Schaffner and I. N. Mishustin, Phys. Rev. C **53**, 1416 (1996); F. Weber, Prog. Part. Nucl. Phys. **54**, 193 (2005).
 - [2] J. M. Lattimer and M. Prakash, Phys. Rep. **442**, 109 (2007); arXiv:1012.3208 (2010).
 - [3] P. Demorest, et al., Nature **467**, 1081 (2010).
 - [4] M. Alford et al., Astrophys. J. **629**, 969 (2005); J. R. Stone et al., Nucl. Phys. A **792**, 341 (2007); A. Kurkela, P. Romatschke, and A. Vuorinen, Phys. Rev. D **81**, 105021 (2010); S. Weissenborn, et al., arXiv:1102.2869 (2011).
 - [5] K. Nakazato, K. Sumiyoshi, and S. Yamada, Phys. Rev. D **77**, 103006 (2008); Astrophys. J. **721**, 1284 (2010).
 - [6] I. Sagert et al., Phys. Rev. Lett. **102**, 081101 (2009); T. Fischer et al., Astrophys. J. Suppl. **194**, 39 (2011).
 - [7] K. Sumiyoshi et al., Astrophys. J. Lett. **690**, L43 (2009).
 - [8] A. Bauswein et al., Phys. Rev. Lett. **103**, 011101 (2009); A. Bauswein, et al., Phys. Rev. D **81**, 024012 (2010).
 - [9] K. Hotokezaka et al., Phys. Rev. D **83**, 124008 (2011).
 - [10] A. Bauswein and H.-T. Janka, arXiv:1106.1616 (2011).
 - [11] C. Ishizuka et al., J. Phys. G **35**, 085201 (2008).
 - [12] J. Abadie, et al., Nucl. Instrum. Methods Phys. Res. Sect. **A624**, 223 (2010); T. Accadia, et al., Class. Quantum Grav. **28**, 025005 (2011); K. Kuroda, et al., Class. Quantum Grav. **27**, 084004 (2010).
 - [13] H. Noumi, et al. Phys. Rev. Lett. **89** 072301 (2002).
 - [14] H. Shen et al., arXiv:1105.1666, (2011); H. Shen, F. Yang, and H. Toki, Prog. Theor. Phys. **115**, 325 (2006).
 - [15] Y. Sekiguchi et al., Phys. Rev. Lett. **107**, 051102 (2011).
 - [16] K. Kiuchi, et al., Phys. Rev. D **80**, 064037 (2009).
 - [17] M. Shibata and T. Nakamura, Phys. Rev. D **52**, 5428 (1995); T. W. Baumgarte and S. L. Shapiro, Phys. Rev. D **59**, 024007 (1998); M. Campanelli, et al., Phys. Rev. Lett. **96**, 111101 (2006).
 - [18] Y. Sekiguchi, Prog. Theor. Phys. **124**, 331 (2010); Class. Quant. Grav. **27**, 114107 (2010).
 - [19] Y. Sekiguchi and M. Shibata, Astrophys. J. **737**, 6 (2011).
 - [20] H. Shen, et al., Nucl. Phys. A **637**, 435 (1998); Prog. Theor. Phys. **100**, 1013 (1998).
 - [21] M. Shibata, K. Taniguchi, and K. Uryū, Phys. Rev. D **71**, 084021 (2005); M. Shibata and K. Taniguchi, Phys. Rev. D **73**, 064027 (2006).
 - [22] L. Rezzolla et al., Astrophys. J. Lett. **732**, L6 (2011).
 - [23] R. Narayan, B. Paczynski, and T. Piran, Astrophys. J. Lett. **395**, L83 (1992); T. Piran, Rev. Mod. Phys. **76**, 1143 (2005); E. Nakar, Phys. Rep. **442**, 166 (2007).
 - [24] M. Ruffert, H.-Th. Janka, and G. Schäfer, Astron. Astrophys. **311**, 532 (1996); M. Ruffert and H.-Th. Janka,

- ibid* **380**, 544 (2001); S. Rosswog and M. Liebendörfer, Mon. Not. R. Astron. Soc. **342**, 673 (2003).
- [25] N. Stergioulas, et al., arXiv:1105.0368 (2011); N. Anderson and K. D. Kokkotas, Mon. Not. R. Astron. Soc. **299**, 1059 (1998).